Available online at www.sciencedirect.com
ScienceDirect
Physica A 387 (2008) 3480–3494
PHYSICA A
www.elsevier.com/locate/physa

Tachyonic γ-ray wideband of an ultra-relativistic electron plasma: Spectral fitting with Fermi power-law densities

Roman Tomaschitz*

Department of Physics, Hiroshima University, 1-3-1 Kagami-yama, Higashi-Hiroshima 739-8526, Japan

Received 28 September 2007; received in revised form 14 January 2008
Available online 15 February 2008

Abstract

Fermionic power-law distributions are derived by the second quantization of classical power-law ensembles, and applied to ultra-relativistic electron populations in the Galactic center. The γ-ray flux from the direction of the compact central source Sagittarius A* is fitted with a superluminal cascade spectrum. In this way, estimates of the radiating electron plasma in the Galactic center region are obtained, such as the power-law index, temperature, particle number, and internal energy. The spectral averaging of the tachyonic radiation densities with Fermi power-laws is explained. Fugacity expansions of the thermodynamic variables (thermal equation of state, entropy, isochoric heat capacity, and isothermal compressibility) are obtained in the quasiclassical high-temperature/low-density regime, where the spectral fit is carried out. The leading quantum correction to these variables is calculated, and its dependence on the electronic power-law index and the thermal wavelength is discussed. Excess counts of cosmic rays from the Galactic center region are related to the plasma temperature inferred from the cascade fit.

PACS: 05.30.Fk; 05.70.Ce; 52.25.Kn; 95.30.Tg

Keywords: Superluminal radiation; Tachyonic cascade spectra; Fermi power-law ensembles; Ultra-relativistic electron plasma; Quasiclassical fugacity expansion; Spectral averaging

1. Introduction

Electronic power-law distributions are commonly used in electromagnetic spectral averages to model the synchrotron emission of astrophysical sources, such as the X-ray spectra of supernova remnants [1]. In this article, we quantize Boltzmann power-law densities, exponentially cut power-law distributions $\mathrm{d}\rho_{\mathrm{B}} \propto H^{-\delta}\mathrm{e}^{-H/(k_{\mathrm{B}}T)}\mathrm{d}^3p$, where $H = mc^2\gamma$ is the free electronic Hamiltonian. In Fermi–Dirac statistics, we arrive at densities

$$\mathrm{d}\rho_F(\gamma) = \frac{m^3c^3V}{\hbar^3\pi^2}\frac{\sqrt{\gamma^2-1}\gamma\mathrm{d}\gamma}{1+\gamma^\delta\mathrm{e}^{\beta\gamma+\alpha}}, \tag{1.1}$$

where the momentum integration has been parametrized with the electronic Lorentz factor γ. δ is the power-law index, and we use the shortcuts $\beta = mc^2/(k_{\mathrm{B}}T)$ and $\alpha = -\beta\mu/(mc^2)$, where μ is the chemical potential. Electronic

* Tel.: +81 824 247361; fax: +81 824 240717.
E-mail address: tom@geminga.org.

0378-4371/$ - see front matter © 2008 Elsevier B.V. All rights reserved.
doi:10.1016/j.physa.2008.02.024

and protonic power-law densities have been invoked to perform electromagnetic and hadronic spectral fits to various TeV γ-ray sources recently discovered with imaging air Cherenkov detectors [2]. Tachyonic spectral fits to the cascade spectra of γ-ray pulsars and microquasars are based on electronic power-law averages as well [3,4]. Power-law indices inferred from these spectral fits or, for that matter, from the magnetospheric radio emission of planets [5,6], usually range in the interval $0 \leqslant \delta \leqslant 4$.

Here, we give evidence for superluminal radiation from the Galactic center by fitting recently obtained spectral maps [7–9] with tachyonic cascade spectra. The tachyonic γ-ray wideband consists of two cascades generated by ultra-relativistic electron populations, and the spectral fit allows us to infer the thermodynamic parameters. The observed spectra are clearly distinguishable from electromagnetic synchrotron and inverse-Compton fits, due to the emergence of extended spectral plateaus. We show that the TeV spectral map of the Galactic center admits a tachyonic extension into the GeV region, providing an excellent fit to the spectrum of the unidentified γ-ray source 3EG J1746 − 2851 [10] associated with the Galactic central source Sagittarius A*. The superluminal cascades are generated by an ultra-relativistic electron gas at high temperature and low density, so that we can use distribution (1.1) in the quasiclassical regime to calculate the thermodynamic variables and the spectral averages.

In Section 2, we set up the thermodynamic formalism of fermionic power-law densities (1.1). Starting with the grand partition function, we derive the quasiclassical fugacity expansion of the thermodynamic variables, such as the caloric and thermal equations of state, entropy, specific heat, and compressibility. In Section 3, we discuss the leading quantum correction to the classical thermodynamic functions. In the high-temperature regime, the quantum corrections become more pronounced with increasing electronic power-law index, exhibiting the same temperature scaling as the classical limit usually dominant in the high-temperature/low-density regime. This is illustrated by calculating the mentioned variables for an increasing sequence of electron indices. We study the thermal wavelength of fermionic power-law ensembles in the low- and high-temperature regime, and discuss the range of applicability of the quasiclassical fugacity expansion.

In Section 4, we average the quantized superluminal radiation densities with the power-law distributions (1.1), and derive the fugacity expansion of the spectral averages. We perform a tachyonic cascade fit to the γ-ray spectrum of the Galactic center, and obtain estimates of the thermodynamic parameters of the electron plasma generating the superluminal radiation. The cutoff energy of the high-energy cascade fitting the TeV spectrum can be related to anisotropies in the cosmic ray spectrum detected by the AGASA and SUGAR air shower arrays [11,12]. If the TeV cascade is generated by a protonic source population, this requires a thermal proton density at $k_{\mathrm{B}}T \approx 10^{18.4}$ eV. This cutoff temperature very closely matches the upper energy edge of both the AGASA and SUGAR excess counts from the Galactic center region, suggesting that the compact radio source Sagittarius A* is capable of accelerating protons into the 10^{18} eV region. In Section 5, we present our conclusions.

2. Thermodynamic variables of Fermi power-law ensembles

We start with the fermionic partition function,

$$\log Z = 2V \int \log\left(1 + \rho(H)\right) \frac{\mathrm{d}^3 p}{(2\pi)^3}, \tag{2.1}$$

where $\rho(H)$ stands for density

$$\rho := \theta(H - H_1)(H/m)^{-\delta} \exp\left(-\beta \frac{H}{m} - \alpha\right), \tag{2.2}$$

and $H = m\gamma$ is the free Hamiltonian. The electronic Lorentz factors $\gamma = (1 - \upsilon^2)^{-1/2}$ range in an interval $\gamma_1 \leqslant \gamma < \infty$. $H_1 = m\gamma_1$ is the lower threshold energy, and $\gamma_1 \geq 1$ the lower edge of Lorentz factors of the electron distribution. The momentum parametrization is $p = m\sqrt{\gamma^2 - 1}$, so that we can substitute $\mathrm{d}^3 p = 4\pi m^3 \sqrt{\gamma^2 - 1}\gamma \mathrm{d}\gamma$, where the angular integration has already been performed, as there is no angular dependence in the integrand. The Heaviside step function θ restricts the $\mathrm{d}^3 p$ integration in (2.1) to $\gamma \geq \gamma_1$. The exponent α defines the fugacity $z = \mathrm{e}^{-\alpha}$, and is related to the chemical potential by $\mu = -m\alpha/\beta$, cf. after (2.26). δ is the electronic power-law exponent, and $\beta = m/(k_{\mathrm{B}}T)$ the cutoff parameter in the Boltzmann factor, so that the relativistic Fermi–Dirac distribution is recovered with $\delta = 0$ and $\gamma_1 = 1$. Here, we study power-law ensembles of arbitrary real power-law index δ. We use

$c = \hbar = 1$ for most of this article; the units can easily be restored, e.g., $\beta = mc^2/(k_{\rm B}T)$, where the ratio of electron rest energy and Boltzmann constant is $mc^2/k_{\rm B} \approx 5.930 \times 10^9$ K.

The grand partition function (2.1) is obtained via a standard trace calculation in fermionic occupation number representation,

$$Z = \mathrm{Tr}_{\omega\geq H_1}\left((\hat{H}/m)^{-\delta}\exp(-\beta\hat{H}/m - \alpha\hat{N})\right), \tag{2.3}$$

where $\mathrm{Tr}_{\omega\geq H_1}$ refers to the trace over multi-particle states with occupation energies ω exceeding the lower threshold $\omega_1 := H_1$. We briefly sketch the derivation of partition function (2.1) from the trace (2.3). A basis $|n\rangle$ for the occupation number representation of the fermionic creation/annihilation operators $b_{\mathbf{k}}^{(+)}$ (labeled by the wave vector $\mathbf{k}$) is explicitly defined in Eq. (4.11) in Ref. [13]. In (2.3), we substitute the particle number operator $\hat{N} := \sum_{|\mathbf{k}|\geq k_1}\hat{N}_{\mathbf{k}}$, where $\hat{N}_{\mathbf{k}} := b_{\mathbf{k}}^+ b_{\mathbf{k}}$, as well as the energy operator $\hat{H} := \sum_{|\mathbf{k}|\geq k_1}\hat{H}_{\mathbf{k}}$, where $\hat{H}_{\mathbf{k}} := \omega_{\mathbf{k}}\hat{N}_{\mathbf{k}}$. In occupation number representation, the Hermitian number operators are diagonal, $\hat{N}_{\mathbf{k}}|n\rangle = n_{\mathbf{k}}|n\rangle$, and the fermionic occupation numbers $n_{\mathbf{k}}$ attached to a wave vector $\mathbf{k}$ can only take the values zero and one. We also note the dispersion relation $\omega_{\mathbf{k}} = \sqrt{k^2+m^2}$, relating electron energy and wave number $k = |\mathbf{k}|$. Finally, $k_1 := m\sqrt{\gamma_1^2-1}$ is the wave number corresponding to the lower threshold energy $\omega_1 = m\gamma_1$.

We employ box quantization, discretizing the wave vector as $\mathbf{k} = 2\pi\mathbf{n}/L$. The following summations are taken over integer lattice points $\mathbf{n}$ in R^3, corresponding to periodic boundary conditions on a box of size L^3. By making use of $\hat{N}_{\mathbf{k}}|n\rangle = n_{\mathbf{k}}|n\rangle$, we may write trace (2.3) over the basis states $|n\rangle$ as

$$\begin{aligned} Z &= \sum_{n_{\mathbf{k}}=0,1}\exp\sum_{|\mathbf{k}|\geq k_1}\left(-\beta\frac{\omega_{\mathbf{k}}}{m} - \delta\log\frac{\omega_{\mathbf{k}}}{m} - \alpha\right)n_{\mathbf{k}} \\ &= \prod_{|\mathbf{k}|\geq k_1}\left(1+\exp\left(-\beta\frac{\omega_{\mathbf{k}}}{m} - \delta\log\frac{\omega_{\mathbf{k}}}{m} - \alpha\right)\right). \end{aligned} \tag{2.4}$$

We thus find

$$\log Z = \sum_{|\mathbf{k}|\geq k_1}\log\left(1+(\omega_{\mathbf{k}}/m)^{-\delta}\exp\left(-\beta\frac{\omega_{\mathbf{k}}}{m} - \alpha\right)\right). \tag{2.5}$$

The continuum limit $L\to\infty$ amounts to replacing the summation over the lattice wave vectors by the integration $2V\int_{|\mathbf{k}|\geq k_1}\mathrm{d}^3k/(2\pi)^3$ [14]; the factor of two accounts for the spin degeneracy. As we have put $\hbar = c = 1$, we can identify $k = p = m\sqrt{\gamma^2-1}$, so that $\omega_{\mathbf{k}} = m\gamma$. Performing these substitutions in (2.5), we arrive at integral representation (2.1) of the partition function, since the Heaviside function in the integrand (2.2) is equivalent to the restriction $p\geq k_1$ of the momentum integration (2.1).

The internal energy,

$$U = -m\frac{\partial}{\partial\beta}\log Z = \frac{m^4V}{\pi^2}\int_{\gamma_1}^{\infty}\frac{\sqrt{\gamma^2-1}\gamma^2\mathrm{d}\gamma}{1+\gamma^\delta \mathrm{e}^{\beta\gamma+\alpha}}, \tag{2.6}$$

and the particle number,

$$N = -\frac{\partial}{\partial\alpha}\log Z = \frac{m^3V}{\pi^2}\int_{\gamma_1}^{\infty}\frac{\sqrt{\gamma^2-1}\gamma\mathrm{d}\gamma}{1+\gamma^\delta \mathrm{e}^{\beta\gamma+\alpha}}, \tag{2.7}$$

are obtained from the integral representation (2.1),

$$\log Z = \frac{m^3V}{\pi^2}\int_{\gamma_1}^{\infty}\log(1+\gamma^{-\delta}\mathrm{e}^{-\beta\gamma-\alpha})\sqrt{\gamma^2-1}\gamma\mathrm{d}\gamma. \tag{2.8}$$

Here we have reparametrized the momentum integration d^3p in (2.1) with the Lorentz factor as explained after (2.2). The integral representations (2.6)–(2.8) are the key ingredients of the Legendre formalism employed below; in particular, $\log Z(\delta,\beta,\alpha,V)$ in (2.8) is the starting point for the quasiclassical fugacity expansion (2.10) (at high

temperature and low density) of the thermodynamic functions. The opposite asymptotic limit, the nearly degenerate quantum regime (low temperature, high density), is based on the representation

$$\log Z = \frac{m^3V}{3\pi^2}\left(\int_{\gamma_1}^{\infty}\frac{(\gamma^2-1)^{3/2}}{1+\gamma^\delta \mathrm{e}^{\beta\gamma+\alpha}}\left(\beta+\frac{\delta}{\gamma}\right)\mathrm{d}\gamma-(\gamma_1^2-1)^{3/2}\log(1+\gamma_1^{-\delta}\mathrm{e}^{-\beta\gamma_1-\alpha})\right), \tag{2.9}$$

where the logarithm in the integrand of (2.8) has been removed by a partial integration. That is, we write the integrand in (2.8) as $f(\gamma)g'(\gamma)/3$, with $f=\log(1+\gamma^{-\delta}\mathrm{e}^{-\beta\gamma-\alpha})$ and $g=(\gamma^2-1)^{3/2}$, and integrate by parts to arrive at (2.9).

For the remainder of this section, we derive the quasiclassical fugacity expansions of the thermodynamic variables. In Section 3, we will discuss the low- and high-temperature limits of these expansions and conditions for their applicability. We start by expanding partition function (2.8) in ascending powers of $\mathrm{e}^{-\alpha}$,

$$\log Z = -\frac{m^3V}{\pi^2}\sum_{n=1}^{\infty}\frac{(-1)^n}{n}\mathrm{e}^{-\alpha n}K(\delta n,\beta n,\gamma_1), \tag{2.10}$$

$$K(\delta,\beta,\gamma_1) := \int_{\gamma_1}^{\infty}\sqrt{\gamma^2-1}\,\gamma^{1-\delta}\mathrm{e}^{-\beta\gamma}\mathrm{d}\gamma, \tag{2.11}$$

and introduce the shortcuts

$$K_n := K(\delta n,\beta n,\gamma_1), \qquad K_{n,j} := K(\delta n-j,\beta n,\gamma_1), \tag{2.12}$$

so that $K_1=K$ and $K_n=K_{n,0}$. Differentiation with respect to β is denoted by a prime, $K'_{n,j}=-nK_{n,j+1}$. The fugacity expansions of the partition function, internal energy, and particle number thus read

$$\log Z = \frac{m^3V}{\pi^2}\mathrm{e}^{-\alpha}K_1\left(1-\frac{\mathrm{e}^{-\alpha}}{2}\frac{K_2}{K_1}+\frac{\mathrm{e}^{-2\alpha}}{3}\frac{K_3}{K_1}-\cdots\right), \tag{2.13}$$

$$U = \frac{m^4V}{\pi^2}\mathrm{e}^{-\alpha}K_{1,1}\left(1-\mathrm{e}^{-\alpha}\frac{K_{2,1}}{K_{1,1}}+\mathrm{e}^{-2\alpha}\frac{K_{3,1}}{K_{1,1}}-\cdots\right), \tag{2.14}$$

$$N = \frac{m^3V}{\pi^2}\mathrm{e}^{-\alpha}K_1\left(1-\mathrm{e}^{-\alpha}\frac{K_2}{K_1}+\mathrm{e}^{-2\alpha}\frac{K_3}{K_1}-\cdots\right). \tag{2.15}$$

We eliminate the fugacity in the partition function and the internal energy by inverting $N(\mathrm{e}^{-\alpha})$ in (2.15):

$$\mathrm{e}^{-\alpha} = \hat{n}\left(1+\frac{K_2}{K_1}\hat{n}+\left(2\frac{K_2^2}{K_1^2}-\frac{K_3}{K_1}\right)\hat{n}^2+O(\hat{n}^3)\right), \tag{2.16}$$

with expansion parameter

$$\hat{n} := \frac{\pi^2}{m^3K_1}\frac{N}{V}. \tag{2.17}$$

The following expansions are ascending series in $\hat{n}$. On substituting (2.16) into (2.13) and (2.14), we find the fugacity expansion of the partition function in Helmholtz parametrization

$$\frac{1}{N}\log Z(\delta,\beta,V,N) = 1+\frac{1}{2}\frac{K_2}{K_1}\hat{n}+\left(\frac{K_2^2}{K_1^2}-\frac{2}{3}\frac{K_3}{K_1}\right)\hat{n}^2+\cdots, \tag{2.18}$$

as well as the internal energy

$$U(\delta,\beta,V,N) = U_{cl}(1+u_1\hat{n}+u_2\hat{n}^2+\cdots), \qquad \frac{U_{cl}}{mN} := \frac{K_{1,1}}{K_1} = -\frac{\partial\log K}{\partial\beta}. \tag{2.19}$$

U_{cl} is the classical limit, the internal energy of a Boltzmann power-law density [4], and the first two series coefficients in (2.19) read

$$u_1 := \frac{K_2}{K_1} - \frac{K_{2,1}}{K_{1,1}}, \qquad u_2 := 2\frac{K_2}{K_1}u_1 - \left(\frac{K_3}{K_1} - \frac{K_{3,1}}{K_{1,1}}\right). \tag{2.20}$$

The fugacity expansion of the entropy function

$$S(\delta, \beta, V, N) = k_{\mathrm{B}} N \left(\frac{\log Z}{N} + \beta\frac{U}{mN} + \alpha\right), \tag{2.21}$$

is obtained by substituting the ascending $\hat{n}$-series (2.18), (2.19), and, cf. (2.16),

$$\alpha = -\log\hat{n} - \frac{K_2}{K_1}\hat{n} - \left(\frac{3}{2}\frac{K_2^2}{K_1^2} - \frac{K_3}{K_1}\right)\hat{n}^2 + O(\hat{n}^3). \tag{2.22}$$

We find

$$\frac{S}{k_{\mathrm{B}}N} = \frac{S_{cl}}{k_{\mathrm{B}}N} + \left(\beta\frac{K_{1,1}}{K_1}u_1 - \frac{1}{2}\frac{K_2}{K_1}\right)\hat{n} + \left(\beta\frac{K_{1,1}}{K_1}u_2 - \frac{1}{2}\frac{K_2^2}{K_1^2} + \frac{1}{3}\frac{K_3}{K_1}\right)\hat{n}^2 + \cdots, \tag{2.23}$$

where the coefficients $u_{1,2}$ are defined in (2.20), and

$$\frac{S_{cl}}{k_{\mathrm{B}}N} = -\log\hat{n} + 1 + \beta\frac{K_{1,1}}{K_1} = 1 - \log\frac{\pi^2 N}{m^3 V} + \log K - \beta\frac{\partial}{\partial\beta}\log K \tag{2.24}$$

is the entropy of a classical Boltzmann power-law density, cf. Ref. [4] and (4.13), with a term $k_{\mathrm{B}}N\log 2$ added owing to the multiplicity factor in (2.1).

The thermal equation of state is derived from the Helmholtz free energy,

$$F(\delta, \beta, V, N) = U - \frac{m}{k_{\mathrm{B}}\beta}S = -\frac{mN}{\beta}\left(\frac{\log Z}{N} + \alpha\right), \tag{2.25}$$

as $P = -\partial F/\partial V$. By making use of the $\hat{n}$-series (2.18) and (2.22), we obtain

$$PV = \frac{mN}{\beta}\left(1 + \frac{1}{2}\frac{K_2}{K_1}\hat{n} + \left(\frac{K_2^2}{K_1^2} - \frac{2}{3}\frac{K_3}{K_1}\right)\hat{n}^2 + \cdots\right). \tag{2.26}$$

The fugacity expansion of the chemical potential $\mu = \partial F/\partial N = -m\alpha/\beta$ is found by substituting the series expansion (2.22) of α.

The isochoric specific heat and the isothermal compressibility are

$$C_V = -\beta\frac{\partial}{\partial\beta}S(\delta, \beta, V, N), \qquad \kappa_T = -\frac{1}{V}\frac{\partial}{\partial P}V(\delta, \beta, P, N), \tag{2.27}$$

where $V(\delta, \beta, P, N)$ is obtained by solving the thermal equation (2.26). As for the heat capacity, we find the fugacity expansion by substitution of (2.23) and (2.24)

$$\frac{C_V}{k_{\mathrm{B}}N} = \frac{C_{V,cl}}{k_{\mathrm{B}}N} - \beta\frac{\partial}{\partial\beta}\left(\beta\frac{K_{1,1}}{K_1}u_1\hat{n} - \frac{1}{2}\frac{K_2}{K_1}\hat{n}\right) + O(\hat{n}^2), \tag{2.28}$$

where $C_{V,cl}$ denotes the classical limit

$$\frac{C_{V,cl}}{k_{\mathrm{B}}N} = \beta^2\frac{\partial^2}{\partial\beta^2}\log K. \tag{2.29}$$

To obtain the quantum correction of the isothermal compressibility, we have to iteratively solve (2.26) for V (since $\hat{n} \propto 1/V$, cf. (2.17)),

$$V = \frac{mN}{\beta P}\left(1 + \frac{\pi^2}{2}\frac{K_2}{K_1^2}\frac{\beta P}{m^4} + \cdots\right), \qquad \kappa_T = \kappa_{T,cl}\left(1 - \frac{\pi^2}{2}\frac{K_2}{K_1^2}\frac{\beta P}{m^4} + \cdots\right), \tag{2.30}$$

where $\kappa_{T,cl} = 1/P$ is the classical limit. Thermodynamic stability requires $C_V \geq 0$ and $\kappa_T \geq 0$. The leading order of the fugacity expansion of C_V in (2.28) and κ_T in (2.30) is in either case positive, as it coincides with the classical limit based on a Boltzmann power-law density [4].

3. Equations of state, entropy, and heat capacity of fermionic power-law densities in the quasiclassical regime

3.1. Low-temperature asymptotics

In the quasiclassical regime covered by the fugacity expansions in Section 2, the low-temperature limit of the thermodynamic variables is determined by the $\beta \gg 1$ asymptotics of integral $K(\delta, \beta, \gamma_1)$ in (2.11). At $\gamma_1 = 1$, the asymptotic $1/\beta$-series reads

$$K(\delta, \beta, 1) = \sqrt{\frac{\pi}{2}}\frac{\mathrm{e}^{-\beta}}{\beta^{3/2}}\left[1 - \frac{1}{\beta}\frac{3}{2}\left(\delta - \frac{5}{4}\right) + \frac{1}{\beta^2}\frac{15}{8}\left(\delta^2 - \frac{3}{2}\delta + \frac{7}{16}\right) + \cdots\right], \tag{3.1}$$

to be substituted into the fugacity expansions of the respective variables, cf. (2.19), (2.23), (2.26), (2.28) and (2.30). In the following, we put $\gamma_1 = 1$ in partition function (2.8). (An ultra-relativistic lower threshold energy can be treated in like manner; the low-temperature expansion of $K(\delta, \beta, \gamma_1 \gg 1)$ is given in Ref. [15].) The series coefficients in the fugacity expansions are composed of certain K-ratios. Using the notation (2.12), we find

$$\frac{K_2}{K_1^2} = \frac{\beta^{3/2}}{2\sqrt{\pi}}\left(1 + \frac{1}{\beta}\left(\frac{3}{2}\delta - \frac{45}{16}\right) + \cdots\right), \tag{3.2}$$

and the same for $K_{2,1}/(K_{1,1}K_1)$, with 45/16 replaced by 57/16. As for coefficient u_1 in (2.20), we note $u_1/K_1 \sim 3\beta^{1/2}/(8\sqrt{\pi})$, up to terms of $O(1/\beta)$. Finally, $K_{1,1}/K_1 \sim 1$ in leading order. Since $\hat{n} \propto 1/K_1$, cf. (2.17), these ratios already suffice to obtain the temperature and density scaling of the leading quantum correction to the thermodynamic variables. The low-temperature limit of the internal energy (2.19) is found as

$$U = U_{cl}\left(1 + \frac{3}{8}\pi^{3/2}\frac{\beta^{1/2}}{m^3}\left(1 + O\left(\frac{1}{\beta}\right)\right)\frac{N}{V} + \cdots\right), \qquad \frac{U_{cl}}{mN} = 1 + \frac{3}{2}\frac{1}{\beta} + O\left(\frac{1}{\beta^2}\right), \tag{3.3}$$

where the ellipsis indicates terms of $O(\hat{n}^2)$, that is, higher orders in N/V. The leading factor U_{cl} is the low-temperature expansion of the internal energy of a classical power-law density [4]. The thermal equation of state (2.26) reads

$$\frac{PV\beta}{mN} = 1 + \frac{1}{4}\pi^{3/2}\frac{\beta^{3/2}}{m^3}\frac{N}{V} + \cdots, \tag{3.4}$$

where the quantum correction $\propto N/V$ stems from the linear $\hat{n}$-term in (2.26). We may replace β by the thermal wavelength, $\lambda_{th} = \sqrt{2\pi\beta}/m$, to find condition $\lambda_{th}^3 N/V \ll 1$ for the quasiclassical fugacity expansion to apply; at low temperatures, the gas has to be sufficiently dilute. The mean kinetic energy per particle in the low-temperature regime is $E_{av} := U/N - m$, so that $\beta \propto m/E_{av}$ in leading order. We thus recover the nonrelativistic wave-mechanical scaling $\lambda_{th} \propto (mE_{av})^{-1/2}$.

The leading quantum correction to entropy, heat capacity, and compressibility scales linearly with density N/V. As for the entropy, cf. (2.23) and (2.24), we find

$$\begin{aligned}\frac{S}{k_B N} &= \frac{S_{cl}}{k_B N} + \frac{1}{8}\pi^{3/2}\frac{\beta^{3/2}}{m^3}\frac{N}{V} + \cdots,\\ \frac{S_{cl}}{k_B N} &= \frac{5}{2} - \log\frac{2^{1/2}\pi^{3/2}N}{m^3 V} - \frac{3}{2}\log\beta - \frac{3}{\beta}\left(\delta - \frac{5}{4}\right) + O\left(\frac{1}{\beta^2}\right),\end{aligned} \tag{3.5}$$

and the specific heat at constant volume reads, cf. (2.28) and (2.29),

$$\frac{C_V}{k_{\rm B}N}=\frac{C_{V,cl}}{k_{\rm B}N}-\frac{3}{16}\pi^{3/2}\frac{\beta^{3/2}}{m^3}\frac{N}{V}+\cdots,\qquad \frac{C_{V,cl}}{k_{\rm B}N}=\frac{3}{2}-\frac{3}{\beta}\left(\delta-\frac{5}{4}\right)+O\left(\frac{1}{\beta^2}\right). \tag{3.6}$$

The classical isothermal compressibility is $\kappa_{T,cl}=1/P$, and the quantum correction is found as, cf. (2.30),

$$\kappa_T=\kappa_{T,cl}\left(1-\frac{1}{4}\pi^{3/2}\frac{\beta^{5/2}}{m^4}P+\cdots\right). \tag{3.7}$$

The series expansions (3.3)–(3.7) are in ascending powers of N/V or P. We have only stated the leading quantum correction, that is, the term linear in N/V or P. The indicated temperature scaling of this term is meant in leading order as well, the next-to-leading order being smaller by a factor of $O(1/\beta)$, cf. (3.3).

3.2. Fugacity expansion and thermal wavelength in the high-temperature limit

Like in Section 3.1, the quasiclassical high-temperature asymptotics of the thermodynamic variables are based on the ascending $\hat{n}$-series ($\hat{n}\propto N/V$) derived in Section 2, namely U in (2.19), S in (2.23), the thermal equation of state (2.26), and C_V in (2.28). As for the compressibility κ_T, we will use the ascending P-series in (2.30). The leading quantum correction to these variables is the term linear in $\hat{n}$ or P, which is in all cases composed of the K-ratios, cf. (2.11) and (2.12),

$$\frac{K_2}{K_1^2}=\frac{K(2\delta,2\beta,1)}{K^2(\delta,\beta,1)},\qquad \frac{K_{1,1}}{K_1}=\frac{K(\delta-1,\beta,1)}{K(\delta,\beta,1)},\qquad \frac{K_{2,1}}{K_{1,1}K_1}=\frac{K(2\delta-1,2\beta,1)}{K(\delta-1,\beta,1)K(\delta,\beta,1)}. \tag{3.8}$$

The high-temperature expansion ($\beta\ll 1$) of these ratios is calculated from the ascending β-series of integral $K(\delta,\beta,1)$ in (2.11), cf. Ref. [15]. The structure of the high-temperature expansion of $K(\delta,\beta,1)$ depends on the power-law index δ. In the following, we list the thermodynamic functions at integer power-law indices $\delta=0,1,\ldots,4$. These indices exhaust all qualitatively different cases; non-integer power-law indices can be dealt with in the same way, based on the β-expansions of $K(\delta,\beta,\gamma_1)$ in Ref. [15], which cover real δ as well as ultra-relativistic threshold Lorentz factors $\gamma_1\gg 1$. In this subsection, we study $\gamma_1=1$ and integer power-law indices $0\leqslant\delta\leqslant 4$.

At $\delta=0$, a thermal Fermi–Dirac distribution is recovered, admitting the quasiclassical high-temperature expansions [14]

$$\begin{aligned}
&\frac{U(\delta=0)}{mN}=\frac{3}{\beta}\left(1+\frac{\pi^2}{32}\frac{\beta^3}{m^3}\frac{N}{V}+\cdots\right),\qquad \frac{PV\beta}{mN}=1+\frac{\pi^2}{32}\frac{\beta^3}{m^3}\frac{N}{V}+\cdots,\\
&\frac{S}{k_{\rm B}N}=4-\log\frac{\pi^2N}{2m^3V}-3\log\beta+\frac{\pi^2}{16}\frac{\beta^3}{m^3}\frac{N}{V}+\cdots,\\
&\frac{C_V}{k_{\rm B}N}=3-\frac{3\pi^2}{16}\frac{\beta^3}{m^3}\frac{N}{V}+\cdots,\qquad \kappa_TP=1-\frac{\pi^2}{32}\frac{\beta^4}{m^4}P+\cdots.
\end{aligned} \tag{3.9}$$

We write here κ_TP for $\kappa_T/\kappa_{T,cl}$, cf. (2.30). The quantum corrections are the terms linear in N/V or P; the logarithms in the expansion of S stem from the classical term S_{cl} in (2.24). At index $\delta=1$, we find

$$\begin{aligned}
&\frac{U(\delta=1)}{mN}=\frac{2}{\beta}\left(1+\frac{3\pi^2}{8}\frac{\beta^3}{m^3}\frac{N}{V}+\cdots\right),\qquad \frac{PV\beta}{mN}=1+\frac{\pi^2}{4}\frac{\beta^3}{m^3}\frac{N}{V}+\cdots,\\
&\frac{S}{k_{\rm B}N}=3-\log\frac{\pi^2N}{m^3V}-2\log\beta+\frac{\pi^2}{2}\frac{\beta^3}{m^3}\frac{N}{V}+\cdots,\\
&\frac{C_V}{k_{\rm B}N}=2-\frac{3\pi^2}{2}\frac{\beta^3}{m^3}\frac{N}{V}+\cdots,\qquad \kappa_TP=1-\frac{\pi^2}{4}\frac{\beta^4}{m^4}P+\cdots.
\end{aligned} \tag{3.10}$$

There is no qualitative difference to the Fermi–Dirac variables (3.9) as yet. The entropy has the usual logarithmic divergence, the heat capacity approaches a finite limit, and the internal energy has a $1/\beta$ divergence. All quantum

corrections vanish for $\beta \to 0$. At $\delta = 2$, we obtain

$$\frac{U(\delta=2)}{mN} = \frac{1}{\beta}\left(1+\frac{\pi^3}{4}\frac{\beta^2}{m^3}\frac{N}{V}+\cdots\right), \qquad \frac{PV\beta}{mN} = 1+\frac{\pi^3}{8}\frac{\beta^2}{m^3}\frac{N}{V}+\cdots,$$
$$\frac{S}{k_{\mathrm{B}}N} = 2-\log\frac{\pi^2 N}{m^3 V}-\log\beta+\frac{\pi^3}{8}\frac{\beta^2}{m^3}\frac{N}{V}+\cdots,$$
$$\frac{C_V}{k_{\mathrm{B}}N} = 1-\frac{\pi^3}{4}\frac{\beta^2}{m^3}\frac{N}{V}+\cdots, \qquad \kappa_T P = 1-\frac{\pi^3}{8}\frac{\beta^3}{m^4}P+\cdots. \tag{3.11}$$

In the thermal equation of state and the compressibility, the quantum correction is augmented by a factor of $1/\beta$ as compared to the previous cases $\delta = 0, 1$, which has implications for the thermal wavelength, cf. after (3.16). The quantum correction to the compressibility is of the same order as in the thermal equation, since $P \sim mN/(\beta V)$.

For index $\delta = 3$, there emerges a logarithmic temperature dependence already in the classical internal energy and heat capacity [4]. Introducing the shortcut

$$l_E(\beta) := \log(2/\beta) - \gamma_E - 1, \tag{3.12}$$

where $\gamma_E \approx 0.5772$ is Euler's constant, we find

$$\frac{U(\delta=3)}{mN} = \frac{1}{\beta l_E(\beta)}\left(1+\frac{\pi^3}{16}\frac{1}{l_E^2(\beta)m^3}\frac{N}{V}+\cdots\right),$$
$$\frac{PV\beta}{mN} = 1+\frac{\pi^3}{32}\frac{1}{l_E^2(\beta)m^3}\frac{N}{V}+\cdots,$$
$$\frac{S}{k_{\mathrm{B}}N} = 1-\log\frac{\pi^2 N}{m^3 V}+\log l_E(\beta)+\frac{1}{l_E(\beta)}-\frac{\pi^3}{32}\frac{l_E(\beta)-2}{l_E^3(\beta)m^3}\frac{N}{V}+\cdots,$$
$$\frac{C_V}{k_{\mathrm{B}}N} = \frac{l_E(\beta)-1}{l_E^2(\beta)}-\frac{\pi^3}{16}\frac{l_E(\beta)-3}{l_E^4(\beta)m^3}\frac{N}{V}+\cdots, \qquad \kappa_T P = 1-\frac{\pi^3}{32}\frac{\beta P}{l_E^2(\beta)m^4}+\cdots. \tag{3.13}$$

The entropy diverges very slowly for $\beta \to 0$, owing to a double-logarithmic divergence. The heat capacity approaches zero logarithmically, but stays positive at finite temperature. The quantum corrections vanish logarithmically, except for κ_T. At $\delta = 4$, the expansions read

$$\frac{U(\delta=4)}{mN} = \frac{4}{\pi}l_E(\beta)\left(1+\left(\frac{\pi}{2}-\frac{8\pi}{15}\frac{1}{l_E(\beta)}\right)\frac{1}{m^3}\frac{N}{V}+\cdots\right),$$
$$\frac{PV\beta}{mN} = 1+\frac{\pi}{4}\frac{1}{m^3}\frac{N}{V}+\cdots,$$
$$\frac{S}{k_{\mathrm{B}}N} = 1-\log\frac{4\pi N}{m^3 V}-\frac{4}{\pi}\beta-\left(\frac{\pi}{4}+2\beta\right)\frac{1}{m^3}\frac{N}{V}+\cdots,$$
$$\frac{C_V}{k_{\mathrm{B}}N} = \frac{4}{\pi}\beta+2\frac{\beta}{m^3}\frac{N}{V}+\cdots, \qquad \kappa_T P = 1-\frac{\pi}{4}\frac{\beta}{m^4}P+\cdots, \tag{3.14}$$

with $l_E(\beta)$ defined in (3.12). In this case, the internal energy diverges logarithmically, and the entropy approaches a finite limit at $\beta = 0$. (For power-law indices $\delta > 4$, the internal energy reaches saturation, attaining a finite limit at $\beta = 0$ like the entropy, since integral (2.6) stays finite without exponential cutoff.) In (3.14), the quantum correction to the thermal equation is in leading order independent of β, approaching the indicated finite limit linear in N/V. The quantum correction to the specific heat has the same linear β-dependence as the classical term, in leading order that is, and both terms are positive. (At $\delta = 5$, the classical term as well as the quantum correction scale $\propto \beta^2 l_E(\beta)$ in leading order, with positive proportionality constants.)

In the fugacity expansions (3.9)–(3.14), the quantum correction is the term linear in N/V (or P in the case of $\kappa_T P$). Only the leading order in β is indicated, in the classical term as well as the quantum correction, except for the entropy function in (3.14), where the next-to-leading order in β is included in the quantum correction, so that the

heat capacity can be recovered by differentiation, cf. (2.27). Otherwise, the omitted β-terms are by at least a factor of $O(\beta\log\beta)$ smaller than the indicated ones. (In the expansion procedure, the logs are treated as constants.) The ellipses in expansions (3.9)–(3.14) indicate higher-order quantum corrections in powers of N/V. The units are restored by replacing m by mc^2 on the left-hand side of the above equations as well as in β, cf. after (2.2); on the right-hand side, m is replaced by $mc/\hbar$.

As mentioned after (3.8), high-temperature expansions at a non-integer power-law exponent δ are calculated analogously, by making use of ratios (3.8) and the expansions of $K(\delta,\beta,1)$ in Ref. [15]. High-temperature expansions of thermodynamic variables are differently structured in different δ-intervals, $n-1<\delta<n$, joining the expansions (3.9)–(3.14) at integer δ. Ultra-relativistic high-temperature expansions of $K(\delta,\beta,\gamma_1\gg 1)$ have been obtained in Ref. [15] as well, to be substituted into the ratios (3.8) in the case of power-law distributions with Lorentz factors exceeding a high-energy threshold, cf. (2.3).

Returning to the thermal equation of state (2.26), we define the thermal wavelength λ_T by writing the leading quantum correction in (2.26) as

$$\frac{1}{2}\frac{K_2}{K_1}\hat{n}=\frac{\lambda_T^3}{2^{7/2}}\frac{N}{V},\qquad \lambda_T:=\frac{1}{m}(2^{5/2}\pi^2K_2/K_1^2)^{1/3}. \tag{3.15}$$

The numerical factor in λ_T is chosen in a way to recover the usual definition, $\lambda_{th}=\sqrt{2\pi\beta}/m$, in the low-temperature limit: $\lambda_T\sim\lambda_{th}$ for $\beta\gg 1$. The numerical proportionality factors in λ_{th} and λ_T are a mere convention; λ_T provides a second length scale to be compared to $(V/N)^{1/3}$, which sets the scale for the quantum correction, the quasiclassical regime being defined by $\lambda_T^3N/V\ll 1$, cf. after (3.4). The high-temperature scaling of λ_T at integer power-law indices $\delta=0,1,\ldots,4$ is

$$\begin{aligned}&\lambda_T(\delta=0,1)\propto\frac{\beta}{m},\qquad \lambda_T(\delta=2)\propto\frac{\beta^{2/3}}{m},\\ &\lambda_T(\delta=3)\propto\frac{1}{l_E^{2/3}(\beta)m},\qquad \lambda_T(\delta=4)\propto\frac{1}{m},\end{aligned} \tag{3.16}$$

where $l_E(\beta)$ denotes the logarithmic temperature dependence (3.12). If $\delta\leqslant 3$, we invert the caloric equation of state to find in leading order, cf. (3.9)–(3.13),

$$\beta_{\delta=0,1,2}\propto\frac{m}{E_{av}},\qquad \beta_{\delta=3}\sim\frac{m}{E_{av}}\frac{1}{l_E(m/E_{av})}, \tag{3.17}$$

where E_{av} stands for the mean particle energy U/N, and $\beta\ll 1$ is implied. On combining (3.16) and (3.17), we find the high-temperature dispersion relation $\lambda_T(E_{av})$. At $\delta=0,1$, we recover the ultra-relativistic wave-mechanical scaling $\lambda_T\propto 1/E_{av}$. For $\delta\geq 4$, the thermal wavelength is proportional to the Compton wavelength, $\lambda_T\propto 1/m$. For intermediate power-law indices, the thermal wavelength is a hybrid of ultra-relativistic and Compton wavelength, e.g., $\lambda_T(\delta=2)\propto m^{-1/3}E_{av}^{-2/3}$.

4. Superluminal γ-rays from the Galactic center: Tachyonic spectral maps and electronic source distributions

In this section, we average tachyonic radiation densities [15] with fermionic power-law distributions, and use the spectral averages to perform a cascade fit to the γ-ray broadband of the Galactic central source Sagittarius A*, cf. Figs. 1 and 2. The thermodynamic parameters of the electron plasma in the Galactic center generating the superluminal cascades are extracted from the spectral fit, cf. Table 1. First we briefly summarize the tachyonic radiation densities, cf. (4.1) and (4.2), then we explain the spectral averaging, in particular the fugacity expansion of the spectral functions and their low- and high-temperature asymptotics, cf. (4.3)–(4.19). The spectral fit in Figs. 1 and 2 is discussed after (4.20).

The quantized tachyonic radiation densities of a uniformly moving spinning charge read [16]

$$p^{\mathrm{T,L}}(\omega,\gamma)=\frac{\alpha_q m_t^2\omega}{\omega^2+m_t^2}\left[\gamma^2-\frac{m_t}{m}\frac{\omega}{m_t}\gamma-\frac{1}{4}\frac{m_t^2}{m^2}-\left(1+\frac{\omega^2}{m_t^2}\right)\Delta^{\mathrm{T,L}}\right]\frac{1}{\gamma\sqrt{\gamma^2-1}}, \tag{4.1}$$

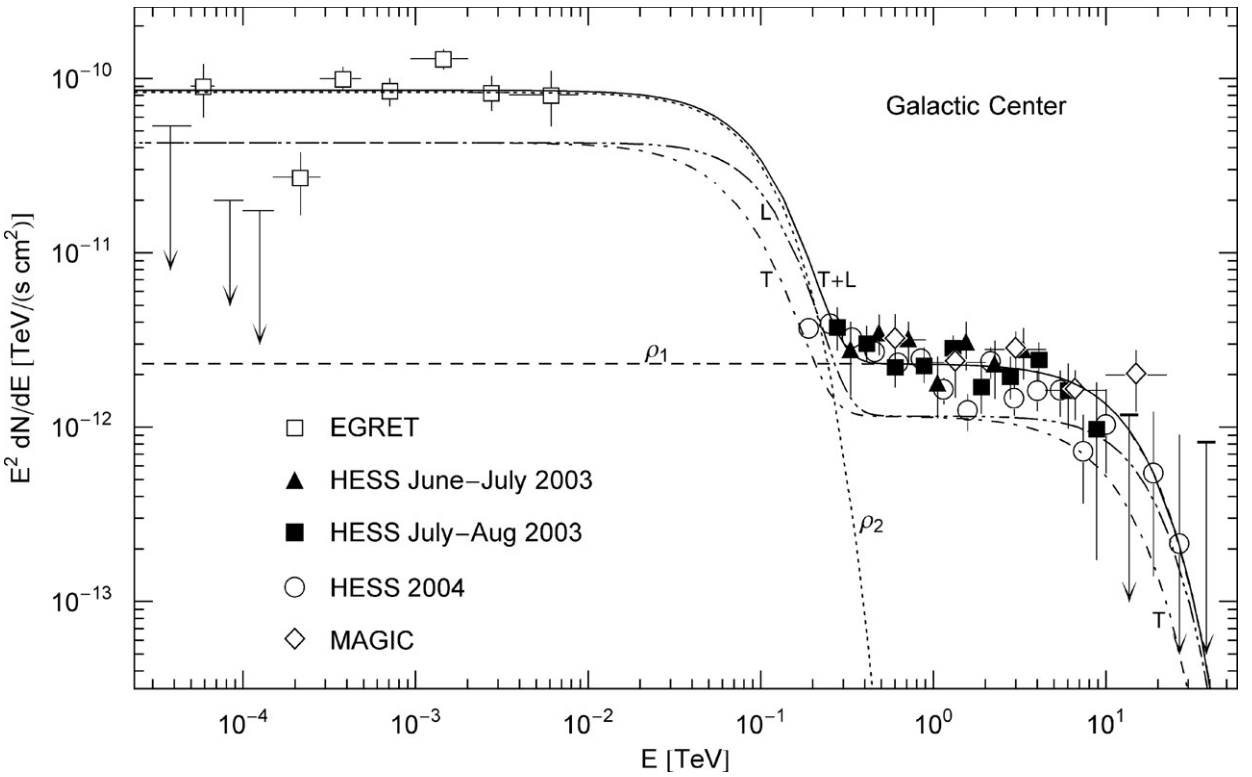

Fig. 1. γ-ray wideband of the Galactic center. EGRET data points from Ref. [2], HESS points from Refs. [7,8], MAGIC points from Ref. [9]. EGRET points refer to the source 3EG J1746 − 2851, HESS and MAGIC points to HESS J1745 − 290. The solid line T + L depicts the unpolarized differential tachyon flux $\mathrm{d}N^{\mathrm{T+L}}/\mathrm{d}E$, obtained by adding the flux densities $\rho_{1,2}$ of two electron populations and rescaled with E^2 for better visibility of the spectral curvature, cf. (4.20). The transversal (T, dot-dashed) and longitudinal (L, double-dot-dashed) flux densities $\mathrm{d}N^{\mathrm{T,L}}/\mathrm{d}E$ add up to the total flux T + L. The χ^2-fit is done with the unpolarized tachyon flux T + L, and subsequently split into transversal and longitudinal components. The exponential decay of the cascades $\rho_{1,2}$ sets in at about $E_{cut} \approx (m_t/m)k_{\mathrm{B}}T$, implying cutoffs at 5.5 TeV for the ρ_1 cascade and at 38 GeV for ρ_2, which terminate the spectral plateaus. The unpolarized flux T + L is the actual spectral fit, the parameters of the electron densities are recorded in Table 1.

where the superscripts T and L refer to the transversal/longitudinal polarization components defined by $\Delta^{\mathrm{T}} = 1 - m_t^2/(2m^2)$ and $\Delta^{\mathrm{L}} = 0$. γ is the electronic Lorentz factor, α_q the tachyonic fine structure constant, and m_t the tachyon mass. A spectral cutoff occurs at

$$\omega_{\max}(\gamma) = m_t\left(\mu_t\sqrt{\gamma^2-1} - \frac{1}{2}\frac{m_t}{m}\gamma\right), \quad \mu_t := \sqrt{1+\frac{m_t^2}{4m^2}}. \tag{4.2}$$

Only frequencies in the range $0 \leqslant \omega \leqslant \omega_{\max}(\gamma)$ can be radiated by a uniformly moving charge, the tachyonic spectral densities $p^{\mathrm{T,L}}(\omega,\gamma)$ being cut off at the break frequency $\omega_{\max}$. The units $\hbar = c = 1$ can easily be restored. We use the Heaviside–Lorentz system, so that $\alpha_q = q^2/(4\pi\hbar c) \approx 1.0 \times 10^{-13}$. The tachyon mass is $m_t \approx 2.15$ keV/c^2, and the tachyon–electron mass ratio $m_t/m \approx 1/238$. These estimates are obtained from hydrogenic Lamb shifts [17]. A positive $\omega_{\max}(\gamma)$ requires Lorentz factors exceeding the threshold μ_t in (4.2), since $\omega_{\max}(\mu_t) = 0$. The lower threshold on the speed of the electron for radiation to occur is thus $\upsilon_{\min} := m_t/(2m\mu_t)$. The tachyon–electron mass ratio gives $\upsilon_{\min}/c \approx 2.1 \times 10^{-3}$, cf. Ref. [18].

The radiation densities (4.1) refer to a single charge with Lorentz factor γ. We average them with a Fermi power-law distribution,

$$\mathrm{d}\rho_F(\gamma) = A_F\frac{\sqrt{\gamma^2-1}\gamma\mathrm{d}\gamma}{1+\gamma^\delta \mathrm{e}^{\beta\gamma+\hat{\alpha}}}, \tag{4.3}$$

Table 1
Electronic source densities $\rho_{1,2}$ generating the γ-ray broadband of the TeV source HESS J1745 − 290 and the associated EGRET source 3EG J1746 − 2851 in the Galactic center region

	β	$\hat{n}$	n^{e}@8 kpc	$k_{\mathrm{B}}T$ (TeV)	U (erg)
ρ_1	3.91×10^{-10}	2.5×10^{-4}	9.2×10^{47}	1310	5.8×10^{51}
ρ_2	5.66×10^{-8}	9.0×10^{-3}	3.3×10^{49}	9.0	1.4×10^{51}

Each ρ_i stands for a Maxwell–Boltzmann density $\mathrm{d}\rho_{\alpha=-2,\beta}(\gamma)$, cf. (4.13). β is the cutoff parameter in the Boltzmann factor. $\hat{n}$ determines the amplitude of the tachyon flux generated by ρ_i, from which the electron count $n^{\mathrm{e}} \propto d^2$ is inferred at the indicated distance of 8 kpc, cf. after (4.21). (The subscript 1 in $\hat{n}$ and n^{e} has been dropped.) $k_{\mathrm{B}}T$ is the electron temperature, and U (erg) the internal energy of the thermal densities ρ_i. The cascades labeled $\rho_{1,2}$ in Figs. 1 and 2 are obtained by averaging the tachyonic radiation densities (4.1) with the electron densities ρ_i, cf. (4.14)–(4.16). The parameters β and $\hat{n}$ are extracted from the least-squares fit T + L in Fig. 1.

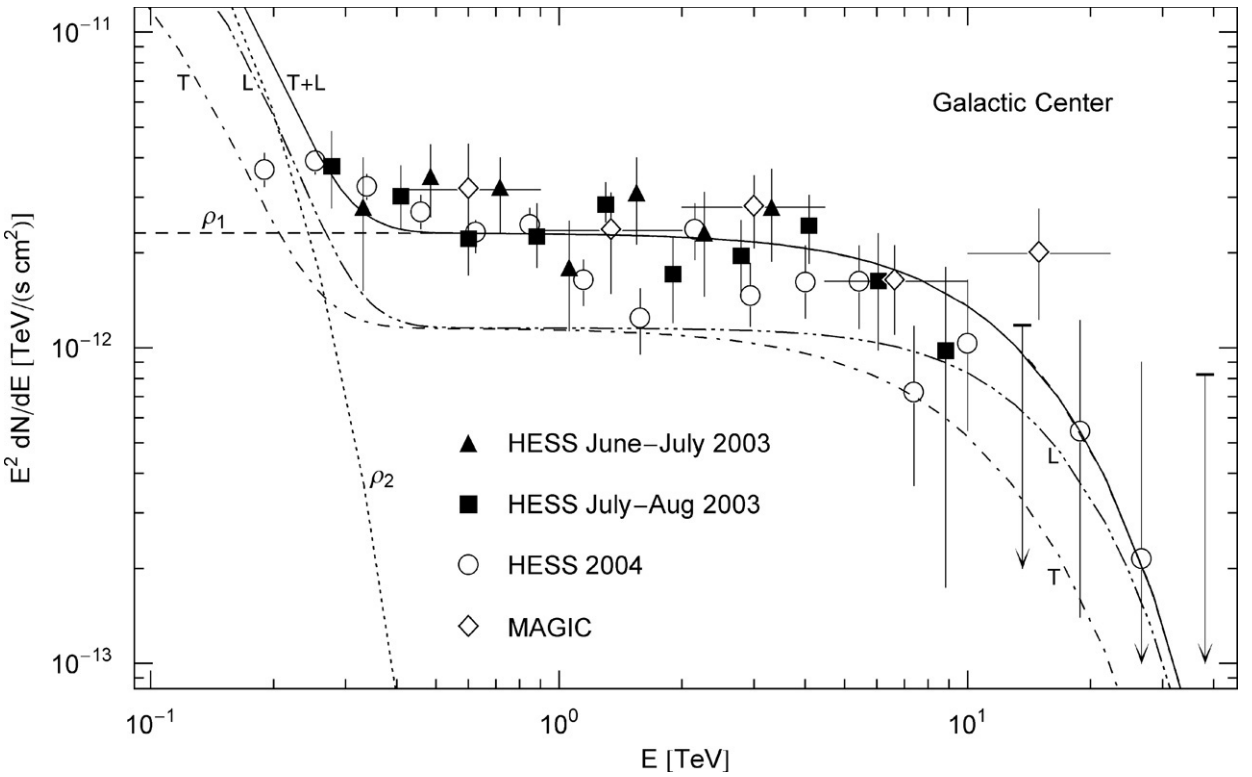

Fig. 2. Close-up of the HESS spectrum in Fig. 1. The TeV spectral map coincides with the ρ_1 cascade, since the ρ_2 flux is exponentially cut at 38 GeV. T and L stand for the transversal and longitudinal flux components, and T + L labels the unpolarized flux. The HESS points define a spectral plateau in the high GeV range typical for tachyonic cascade spectra [15,16]. The spectral curvature is intrinsic, being generated by the Boltzmann factor in the electron densities.

with normalization $A_F := m^3V/\pi^2$, cf. (2.6)–(2.8). The particle number is $N = \int_{\gamma_1}^{\infty} \mathrm{d}\rho_F(\gamma)$, where γ_1 is the lower edge of Lorentz factors in the source population. The exponential cutoff in (4.3) is related to the electron temperature by $\beta = mc^2/(k_{\mathrm{B}}T)$. In this section, we write the exponent of the fugacity $\mathrm{e}^{-\hat{\alpha}}$ with a hat, cf. after (2.2), to distinguish it from the electron index customarily defined as $\alpha = \delta - 2$, cf. (4.13). The normalization factor A_F is dimensionless via $m \to mc/\hbar$, cf. (1.1); the volume factor in the quantum corrections discussed in Section 3 is thus found as $V = \pi^2 \lambda\!\!\!^{-3}_{\mathrm{e}} A_F$, where $\lambda\!\!\!^{-}_{\mathrm{e}} \approx 386$ fm is the reduced electronic Compton wavelength.

The spectral average of the radiation densities (4.1) is carried out as

$$\langle p^{\mathrm{T,L}}(\omega)\rangle_F := \int_{\gamma_1}^{\infty} p^{\mathrm{T,L}}(\omega,\gamma)\theta(\omega_{\max}(\gamma)-\omega)\mathrm{d}\rho_F(\gamma), \tag{4.4}$$

where θ is the Heaviside step function. The spectral range of densities (4.1) is bounded by $\omega_{\max}$, so that the solution of $\omega = \omega_{\max}(\hat{\gamma})$ defines the minimal electronic Lorentz factor for radiation at this frequency,

$$\hat{\gamma}(\omega) = \mu_t\sqrt{1+\frac{\omega^2}{m_t^2}} + \frac{1}{2}\frac{m_t}{m}\frac{\omega}{m_t}. \tag{4.5}$$

The average (4.4) can be reduced to the fermionic spectral functions

$$F^{\mathrm{T,L}}(\omega,\gamma_1) := \int_{\gamma_1}^{\infty} p^{\mathrm{T,L}}(\omega,\gamma)\mathrm{d}\rho_F(\gamma), \tag{4.6}$$

with lower integration boundary $\gamma_1 \geq \mu_t$, cf. after (4.2). The threshold Lorentz factor γ_1 defines the break frequency [19]

$$\omega_1 := \omega_{\max}(\gamma_1) = m_t\left(\mu_t\sqrt{\gamma_1^2-1} - \frac{1}{2}\frac{m_t}{m}\gamma_1\right), \tag{4.7}$$

which separates the spectrum into a low- and high-frequency band. In particular, $\hat{\gamma}(\omega_1) = \gamma_1$, and $\hat{\gamma}(\omega) > \gamma_1$ if $\omega > \omega_1$. By making use of the spectral functions (4.6), we can write the averaged radiation densities (4.4) as

$$\langle p^{\mathrm{T,L}}(\omega)\rangle_F = F^{\mathrm{T,L}}(\omega,\gamma_1)\theta(\omega_1-\omega) + F^{\mathrm{T,L}}(\omega,\hat{\gamma}(\omega))\theta(\omega-\omega_1), \tag{4.8}$$

with $\hat{\gamma}(\omega)$ in (4.5) and ω_1 in (4.7). The superscripts T and L denote the transversal and longitudinal radiation components, cf. (4.1). The spectral functions $F^{\mathrm{T,L}}(\omega,\gamma_1)$ in (4.8) are assembled by substituting the radiation densities (4.1) into the integral representation (4.6),

$$F^{\mathrm{T,L}}(\omega,\gamma_1) = \frac{\alpha_q m_t^2\omega}{\omega^2+m_t^2}\left[f_3(\gamma_1) - \frac{m_t}{m}\frac{\omega}{m_t}f_2(\gamma_1) - \left(\frac{1}{4}\frac{m_t^2}{m^2} + \left(1+\frac{\omega^2}{m_t^2}\right)\Delta^{\mathrm{T,L}}\right)f_1(\gamma_1)\right], \tag{4.9}$$

where the coefficients f_k read

$$f_k(\gamma_1) := \int_{\gamma_1}^{\infty}\frac{\gamma^{k-2}\mathrm{d}\rho_F(\gamma)}{\sqrt{\gamma^2-1}}, \tag{4.10}$$

with density $\mathrm{d}\rho_F(\gamma)$ in (4.3).

The quasiclassical fugacity expansion of the spectral functions (4.9) is found by expanding density (4.3) in ascending powers of $\mathrm{e}^{-\hat{\alpha}}$, cf. (2.10),

$$\mathrm{d}\rho_F(\gamma) \sim A_F\sqrt{\gamma^2-1}\gamma\mathrm{d}\gamma\sum_{n=1}^{\infty}(-1)^{n+1}\gamma^{-\delta n}\mathrm{e}^{-(\beta\gamma+\hat{\alpha})n}, \tag{4.11}$$

so that the asymptotic series of the reduced spectral functions $f_k(\gamma_1)$ in (4.10) reads

$$f_k(\gamma_1) \sim A_F\sum_{n=1}^{\infty}(-1)^{n+1}\gamma_1^{k-\delta n}\mathrm{e}^{-\hat{\alpha}n}\frac{\Gamma(k-\delta n,\beta\gamma_1)}{(\beta\gamma_1)^{k-\delta n}}. \tag{4.12}$$

The classical limit of the fermionic density $\mathrm{d}\rho_F(\gamma)$ is defined by the leading term in series (4.11), the Boltzmann power-law density

$$\mathrm{d}\rho_{\alpha,\beta}(\gamma) := A_{\alpha,\beta}\gamma^{-\alpha-1}\mathrm{e}^{-\beta\gamma}\sqrt{\gamma^2-1}\mathrm{d}\gamma, \tag{4.13}$$

with normalization $A_{\alpha,\beta} := A_F\mathrm{e}^{-\hat{\alpha}}$. (As mentioned after (4.3), exponent $\hat{\alpha}$ in the normalization factor defines the fugacity, and is not to be confused with the electron index $\alpha = \delta - 2$.) The electron count based on the classical density (4.13) is $N = \int_{\gamma_1}^{\infty}\mathrm{d}\rho_{\alpha,\beta}(\gamma)$, to be identified with the renormalized electron count n_1^{e} obtained from the spectral fit, cf. after (4.21).

The classical limit of the fermionic spectral functions $F^{\mathrm{T,L}}(\omega,\gamma_1)$ in (4.6) is the Boltzmann average [15]

$$B^{\mathrm{T,L}}(\omega,\gamma_1) := \int_{\gamma_1}^{\infty} p_{cl}^{\mathrm{T,L}}(\omega,\gamma)\mathrm{d}\rho_{\alpha,\beta}(\gamma). \tag{4.14}$$

Here, $p_{cl}^{\mathrm{T,L}}(\omega,\gamma)$ is the classical spectral density, obtained by dropping all terms containing m_t/m factors in (4.1) and (4.2). In particular, $\Delta_{cl}^{\mathrm{T}}=1$ and $\Delta_{cl}^{\mathrm{L}}=0$, cf. (4.1). Carrying out the integration in (4.14), we find the classical spectral functions

$$B^{\mathrm{T,L}}(\omega,\gamma_1) = A_{\alpha,\beta}\frac{\alpha_q m_t^2\omega}{\omega^2+m_t^2}\beta^{\alpha-1}\left[\Gamma(1-\alpha,\beta\gamma_1) - \left(1+\frac{\omega^2}{m_t^2}\right)\Delta_{cl}^{\mathrm{T,L}}\beta^2\Gamma(-1-\alpha,\beta\gamma_1)\right], \tag{4.15}$$

which can also be obtained from the Fermi functions $F^{\mathrm{T,L}}(\omega,\gamma_1)$ in (4.9) by dropping the m_t/m terms and substituting the leading order of the fugacity expansion of $f_k(\gamma_1)$, cf. (4.12). The classical limit of the fermionic spectral average $\langle p^{\mathrm{T,L}}(\omega)\rangle_F$ in (4.8) thus reads

$$\langle p^{\mathrm{T,L}}(\omega)\rangle_{\alpha,\beta} = B^{\mathrm{T,L}}(\omega,\gamma_1)\theta(\omega_{1,cl}-\omega) + B^{\mathrm{T,L}}\left(\omega,\sqrt{1+\omega^2/m_t^2}\right)\theta(\omega-\omega_{1,cl}), \tag{4.16}$$

where $\omega_{1,cl} := m_t\sqrt{\gamma_1^2-1}$ is the classical limit of the break frequency (4.7).

In the low-temperature limit, $\beta\gamma_1 \gg 1$, the incomplete Γ-functions occurring in the fugacity expansion of $f_k(\gamma_1)$ in (4.12) can be replaced by the asymptotic series

$$\frac{\Gamma(k-\delta n,\beta\gamma_1)}{(\beta\gamma_1)^{k-\delta n}} \sim \frac{\mathrm{e}^{-\beta\gamma_1}}{\beta\gamma_1}\left[1+\frac{k-\delta n-1}{\beta\gamma_1}+\frac{(k-\delta n-1)(k-\delta n-2)}{(\beta\gamma_1)^2}+\cdots\right]. \tag{4.17}$$

At low temperatures, the quasiclassical fugacity expansion can only be used at sufficiently low densities, cf. the discussion of thermal wavelength following (3.4) and (3.15). Spectral averaging at low temperature and high density will be discussed elsewhere. The spectral fit discussed below is carried out in the high-temperature regime, $\beta\gamma_1 \ll 1$. In the fugacity expansion (4.12) of the reduced spectral functions, we can therefore substitute the ascending series

$$\frac{\Gamma(k-\delta n,\beta\gamma_1)}{(\beta\gamma_1)^{k-\delta n}} = (\beta\gamma_1)^{\delta n-k}\Gamma(k-\delta n) - \sum_{l=0}^{\infty}\frac{(-1)^l(\beta\gamma_1)^l}{l!(k-\delta n+l)}. \tag{4.18}$$

If $k-\delta n$ is zero or a negative integer, $k-\delta n=-m$, $m\geq 0$, we use instead of (4.18) the ascending series of the exponential integral $E_{m+1}(\beta\gamma_1)$,

$$\frac{\Gamma(-m,\beta\gamma_1)}{(\beta\gamma_1)^{-m}} = \frac{(-1)^m}{m!}(\beta\gamma_1)^m(\psi(m+1)-\log(\beta\gamma_1)) - \sum_{\substack{l=0\\ l\neq m}}^{\infty}\frac{(-1)^l(\beta\gamma_1)^l}{l!(l-m)}. \tag{4.19}$$

The spectral fit in Figs. 1 and 2 is based on the E^2-rescaled flux densities [20]

$$E^2\frac{\mathrm{d}N^{\mathrm{T,L}}}{\mathrm{d}E} = \frac{\omega}{4\pi d^2}\langle p^{\mathrm{T,L}}(\omega)\rangle_{\alpha,\beta}, \tag{4.20}$$

where d is the distance to the source and $\langle p^{\mathrm{T,L}}(\omega)\rangle_{\alpha,\beta}$ the spectral average (4.16) (with $\omega=E/\hbar$). The fit is done with the unpolarized flux density $\mathrm{d}N^{\mathrm{T+L}}=\mathrm{d}N^{\mathrm{T}}+\mathrm{d}N^{\mathrm{L}}$ of two electron populations $\rho_{i=1,2}$, thermal Maxwell–Boltzmann distributions (4.13) with $\alpha=-2$ and $\gamma_1=1$, cf. Table 1. Each electron density generates a cascade ρ_i, and the wideband fit is obtained by adding two cascade spectra, labeled ρ_1 and ρ_2 in Fig. 1. As for the electron count, $n_1 := \int_1^{\infty}\mathrm{d}\rho_{\alpha,\beta}(\gamma)$, we use a rescaled parameter $\hat{n}_1$ for the fit,

$$\hat{n}_1 := \frac{\alpha_q n_1}{\hbar\ [\mathrm{keV\ s}]4\pi d^2\ [\mathrm{cm}]} \approx 1.27\times 10^{-39}\frac{n_1}{d^2\ [\mathrm{kpc}]}, \tag{4.21}$$

which is independent of the distance estimate in (4.20). Here, $\hbar$ [keV s] implies the tachyon mass in keV units, that is, we put $m_t\approx 2.15$ in the spectral density (4.1). At γ-ray energies, only a tiny $\alpha_q/\alpha_{\mathrm{e}}$-fraction (the ratio of tachyonic

and electric fine structure constants) of the tachyon flux is absorbed by the detector, which requires a rescaling of the electron count n_1, so that the actual number of radiating electrons is $n_1^{\mathrm{e}} := n_1\alpha_{\mathrm{e}}/\alpha_q \approx 7.3\times 10^{10} n_1$. We thus find the electron count to be $n_1^{\mathrm{e}} \approx 5.75\times 10^{49}\hat{n}_1 d^2$ [kpc], where $\hat{n}_1$ defines the tachyonic flux amplitude extracted from the spectral fit [20]. This renormalized count n_1^{e} is to be identified with the particle number N in the thermodynamic variables of the electron plasma. The electron temperature and cutoff parameter in the Boltzmann factor are related by $k_{\mathrm{B}}T$ [TeV] $\approx 5.11\times 10^{-7}/\beta$, and the energy estimates in Table 1 are based on U [erg] $\sim 2.46\times 10^{-6} n_1^{\mathrm{e}}/\beta$, cf. (3.9).

Figs. 1 and 2 show the spectral map of the TeV γ-ray source HESS J1745 − 290 and the GeV source 3EG J1746 − 2851. Both sources are located in the vicinity of the unidentified compact radio source Sagittarius (Sgr) A* at the core of the Galactic center region, which comprises the supernova remnant Sgr A East and the pulsar wind nebula G359.95 − 0.04, as well as molecular cloud complexes such as Sgr B and Sgr C [21,22].

In Table 1, we list the thermodynamic parameters of the electron populations generating the tachyonic cascade spectra $\rho_{1,2}$ depicted in the figures. In the case of protonic source densities (4.13), the cutoff energy $k_{\mathrm{B}}T$ in the Boltzmann factor has to be multiplied by 1.84×10^3, the proton/electron mass ratio, resulting in a cutoff energy of $10^{16.2}$ eV for a protonic ρ_2 population. The protonic high-energy population ρ_1 is cut at $10^{18.4}$ eV, which is to be compared to the excess fluxes from the Galactic center region observed by AGASA in the 10^{18}–$10^{18.4}$ eV range [11], and the SUGAR array in the $10^{17.9}$–$10^{18.5}$ eV interval [12].

The tachyonic spectral maps are further explained in the figure captions, and can be compared to electromagnetic inverse-Compton fits [23] or hadronic fits based on proton–proton scattering and pion decay [2,24]. The electronic source count for the Crab Nebula at $d \approx 2$ kpc is 1.9×10^{50}, cf. Ref. [16], as compared to 3.4×10^{49} for HESS J1745 − 290 and 3EG J1746 − 2851, at a distance of 8 kpc, cf. Table 1. The internal energy of the electron gas is 7.2×10^{51} erg, to be compared to hadronic model estimates predicting 5×10^{45} erg [24], 10^{49}–10^{50} erg [25], and 5.1×10^{50} erg [23] for a protonic source population.

5. Conclusion

We have investigated superluminal radiation from electron populations in the Galactic center region, and found the thermodynamic parameters of the source densities. We demonstrated that the γ-ray wideband of the Galactic center can be fitted with a tachyonic cascade spectrum. In particular, the extended spectral plateau in the MeV–GeV range as well as the spectral curvature apparent in double-logarithmic plots are reproduced by the cascade fit in Figs. 1 and 2. Estimates of the temperature, the source count, and the internal energy of the electron plasma generating the superluminal cascades are given in Table 1.

In Section 4, we averaged the superluminal radiation densities with fermionic power-law distributions, and derived the quantized spectral functions. The power-law densities in Sections 2 and 3 and the spectral averages were studied mostly in the quasiclassical limit, as γ-ray spectral fits are done in the high-temperature regime. The opposite asymptotic limit of nearly degenerate fermionic power-law ensembles at low temperature and high density will be discussed elsewhere.

We quantized Boltzmann power-law densities in Fermi–Dirac statistics, derived the fermionic partition function, developed the Legendre formalism of fermionic power-law distributions, and calculated the fugacity expansion of the thermodynamic variables, cf. Section 2. The qualitative dependence of the variables on the electronic power-law index, the temperature scaling of the quantum corrections, and the thermal wavelength of power-law ensembles were investigated in Section 3. We have focused on γ-ray spectra, which can be fitted with ultra-relativistic electron densities at high temperature, cf. Section 4. As for tachyonic X-ray spectra obtained from diffraction gratings [21], the tachyon mass of 2 keV has to be included in the dispersion relation when parametrizing the glancing angle in the Bragg condition with energy, which affects the shape of the spectral maps in the X-ray bands; this will be discussed elsewhere. The spectral fit in Figs. 1 and 2 is performed with the unpolarized tachyon flux. At γ-ray energies, the speed of tachyons is close to the speed of light, the basic difference to electromagnetic radiation being the longitudinal flux component [26]. The polarization of tachyons can be determined from transversal and longitudinal ionization cross-sections of Rydberg atoms, which peak at different scattering angles [27].

Acknowledgements

The author acknowledges the support of the Japan Society for the Promotion of Science. The hospitality and stimulating atmosphere of the Centre for Nonlinear Dynamics, Bharathidasan University, Trichy, and the Institute of Mathematical Sciences, Chennai, are likewise gratefully acknowledged.

References

[1] S.P. Reynolds, J.W. Keohane, Astrophys. J. 525 (1999) 368.
[2] K. Tsuchiya, et al., Astrophys. J. 606 (2004) L115.
[3] R. Tomaschitz, Astropart. Phys. 27 (2007) 92.
[4] R. Tomaschitz, Physica A 385 (2007) 558.
[5] I. de Pater, B.J. Butler, Icarus 163 (2003) 428.
[6] I. de Pater, et al., Icarus 163 (2003) 434.
[7] F. Aharonian, et al., Astron. Astrophys. 425 (2004) L13.
[8] F. Aharonian, et al., Phys. Rev. Lett. 97 (2006) 221102.
[9] J. Albert, et al., Astrophys. J. 638 (2006) L101.
[10] R.C. Hartman, et al., Astrophys. J. Suppl. 123 (1999) 79.
[11] N. Hayashida, et al., Astropart. Phys. 10 (1999) 303.
[12] J.A. Bellido, et al., Astropart. Phys. 15 (2001) 167.
[13] R. Tomaschitz, Physica A 307 (2002) 375.
[14] S. Chandrasekhar, An Introduction to the Study of Stellar Structure, Dover, New York, 1967.
[15] R. Tomaschitz, Ann. Phys. 322 (2007) 677.
[16] R. Tomaschitz, Eur. Phys. J. C 49 (2007) 815.
[17] R. Tomaschitz, Eur. Phys. J. B 17 (2000) 523.
[18] R. Tomaschitz, Physica A 320 (2003) 329.
[19] R. Tomaschitz, Eur. Phys. J. C 45 (2006) 493.
[20] R. Tomaschitz, Phys. Lett. A 366 (2007) 289.
[21] G. Bélanger, et al., Astrophys. J. 636 (2006) 275.
[22] F. Yusef-Zadeh, et al., Astrophys. J. 656 (2007) 847.
[23] S. Liu, et al., Astrophys. J. 647 (2006) 1099.
[24] D.R. Ballantyne, et al., Astrophys. J. 657 (2007) L13.
[25] F. Aharonian, et al., Nature 439 (2006) 695.
[26] R. Tomaschitz, Eur. Phys. J. D 32 (2005) 241.
[27] R. Tomaschitz, J. Phys. A 38 (2005) 2201.